Electronic Supplementary Information

Rationally Designed Ta_3N_5@ReS_2 Heterojunctions for Promoted Photocatalytic Hydrogen Production

Xiaoqiang Zhan[a,b], Zhi Fang[b], Bing Li[a], Haitao Zhang[b], Leyao Xu[b], Huilin Hou[b*], Weiyou Yang[b*]*

[a] School of Mechanical and Power Engineering, East China University of Science and Technology, Shanghai, 200237, P. R. China.

[b] Institute of Micro/Nano Materials and Devices, Ningbo University of Technology, Ningbo City, 315211, P. R. *China.*

Chemicals:

Tantalum(V) chloride ($TaCl_5$, A.R., Aladdin), glucose (Hushi), ammonium perrhenate (NH_4ReO_4, A.R., Aladdin), thiourea (CH_4N_2S, AR, Hushi, China), hydroxylamine hydrochloride ($HONH_3Cl$, A.R., Aladdin), Sodium sulfide (Na_2S, A.R., Aladdin), sodium sulfate (Na_2SO_3, AR, Hushi), Nafion perfluorinated resin solution (AR, Sigma-aldrich), ethanol (C_2H_6O, AR, Aladdin), and deionized water (Millipore, 18.2 MΩ·cm) was used as chemical reagents without further purification.

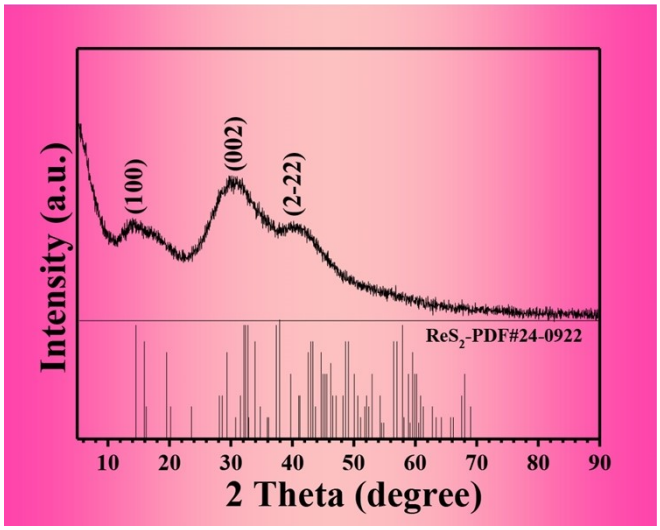

Fig. S1 XRD pattern of pure ReS_2.

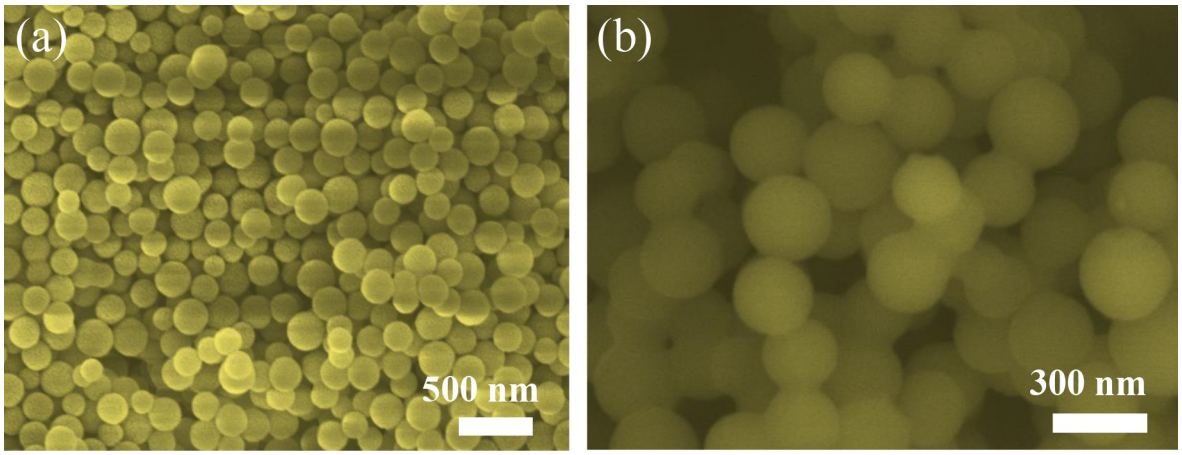

Fig. S2 (a-b) Typical SEM images of the used C balls

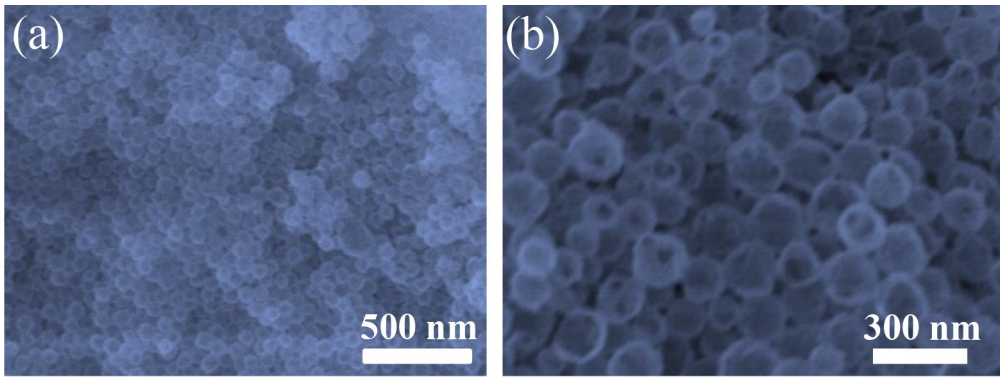

Fig. S3 (a-b) Typical SEM images of TaOx

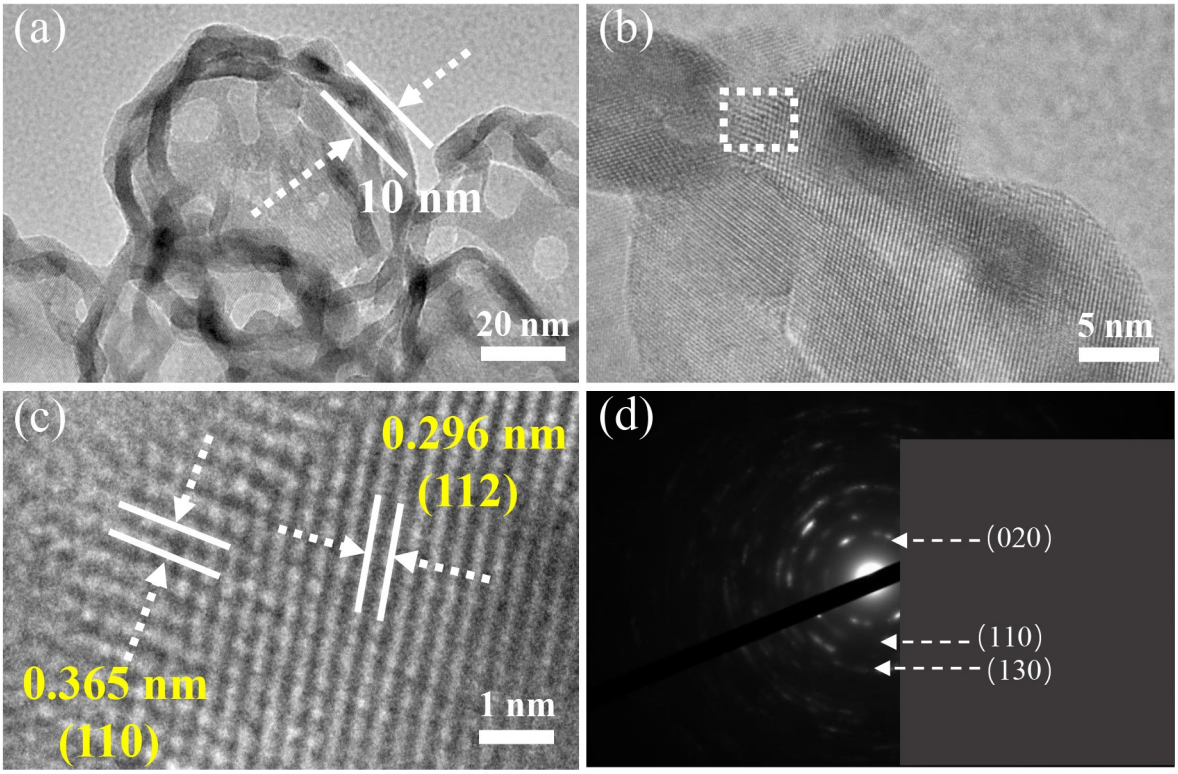

Fig. S4 TEM images (a-b), HRTEM image (c) and SAED pattern (d) of TR0.

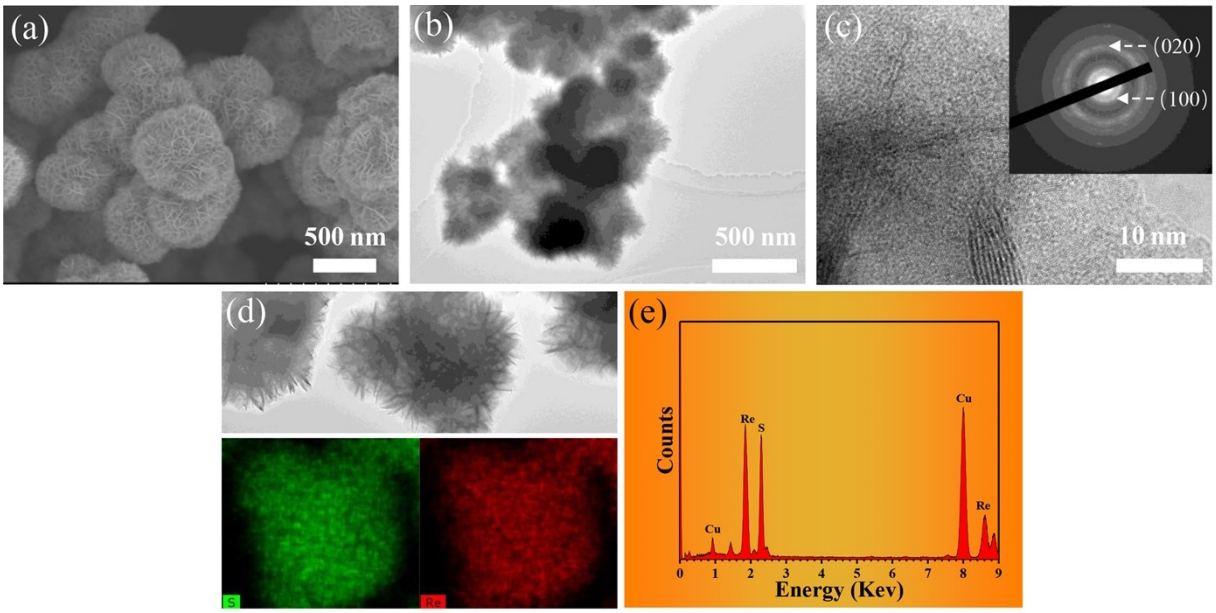

Fig. S5 TEM images (a-b) and HRTEM image (c) of ReS_2, corresponding elemental mapping images (d), and EDX spectrum (e) of ReS_2.

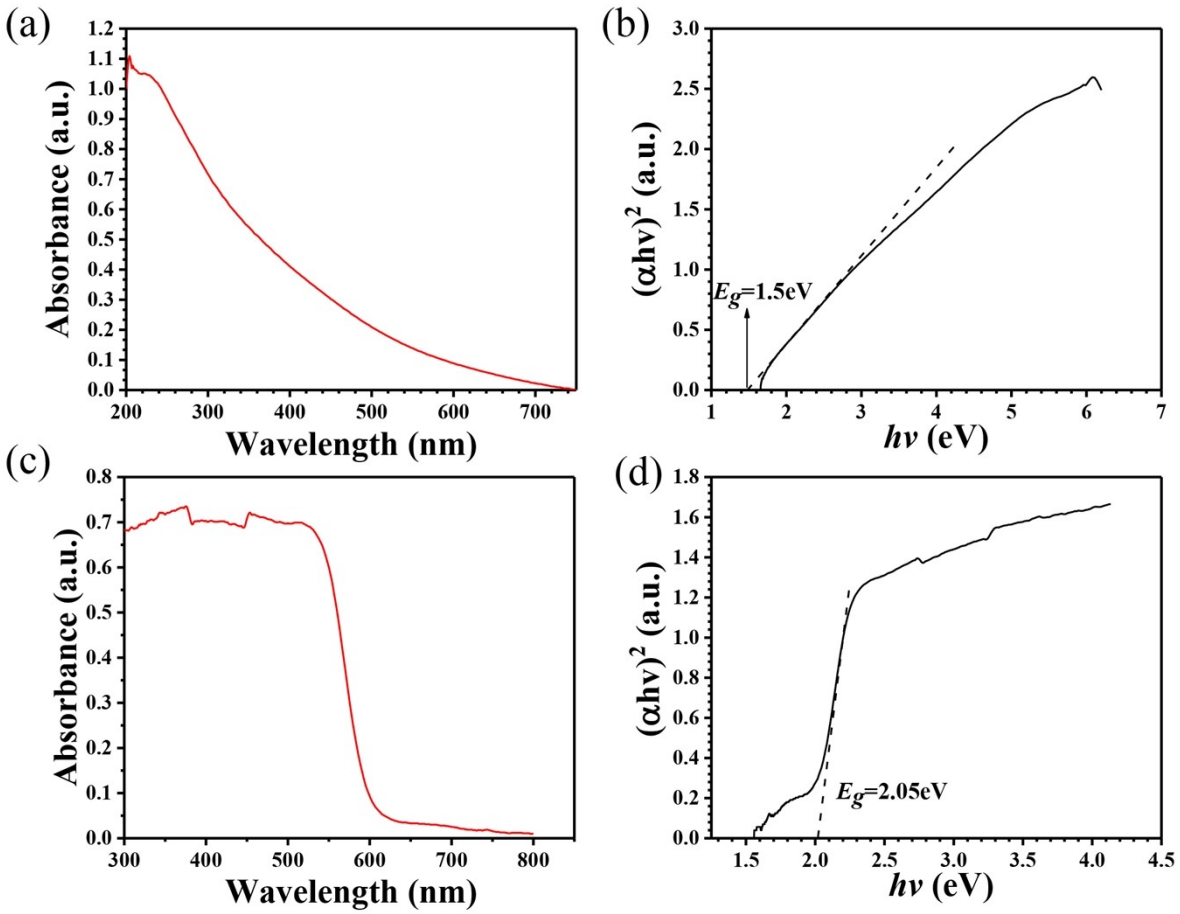

Fig. S6 (a-b) UV-visible absorption spectrum (a) and the calculated bandgap of ReS_2 (b), respectively. (c-d) UV-visible absorption spectrum (c) and the calculated bandgap of TR0 (d), respectively.

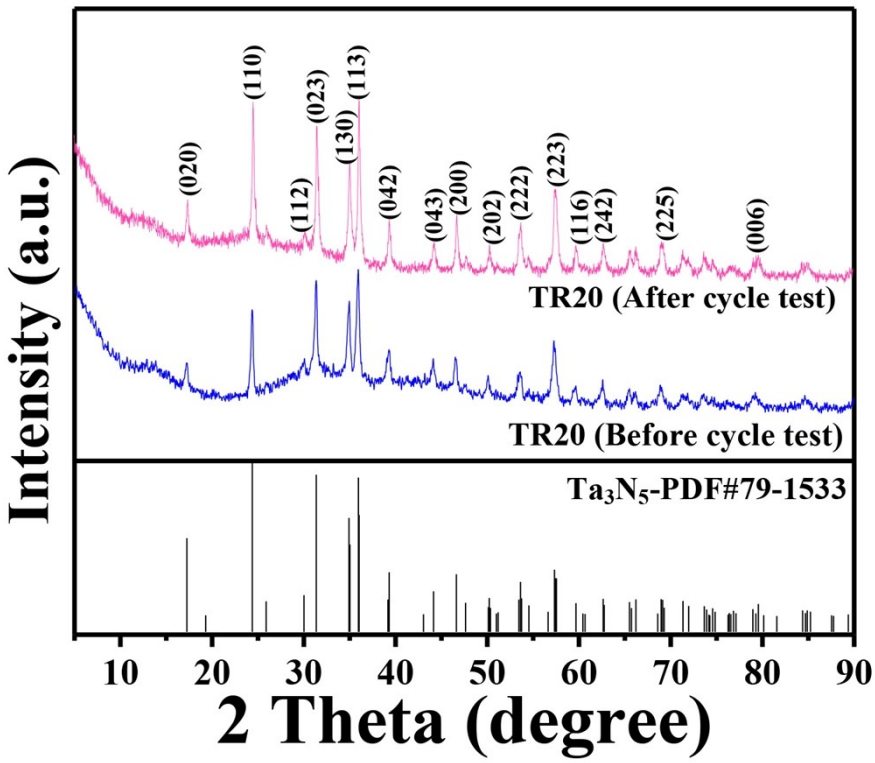

Fig. S7 XRD patterns of TR20 sample before and after cycle test.

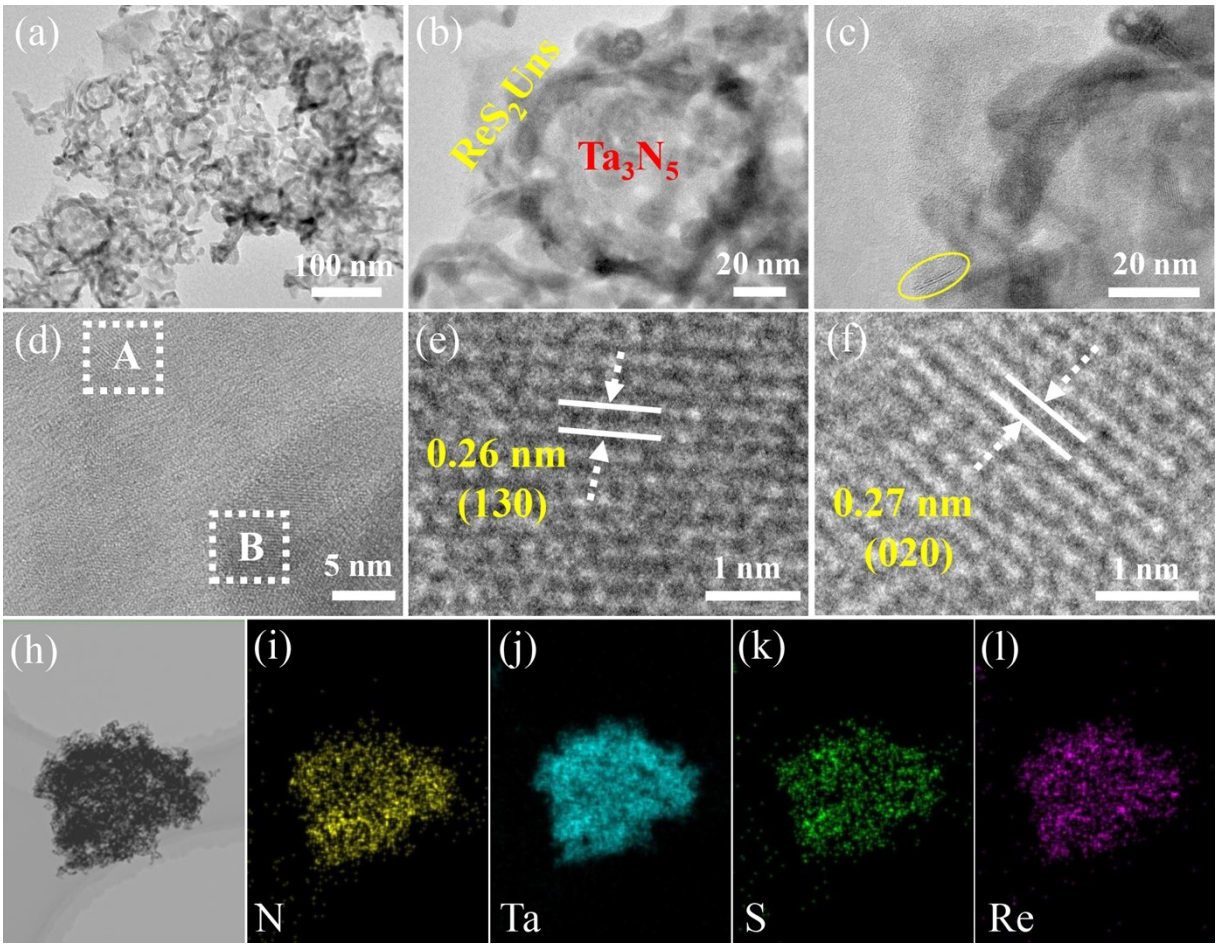

Fig. S8 TEM images (a-c), HRTEM images (d-f) and element mapping images (h-l) of TR20 sample after cycle test.

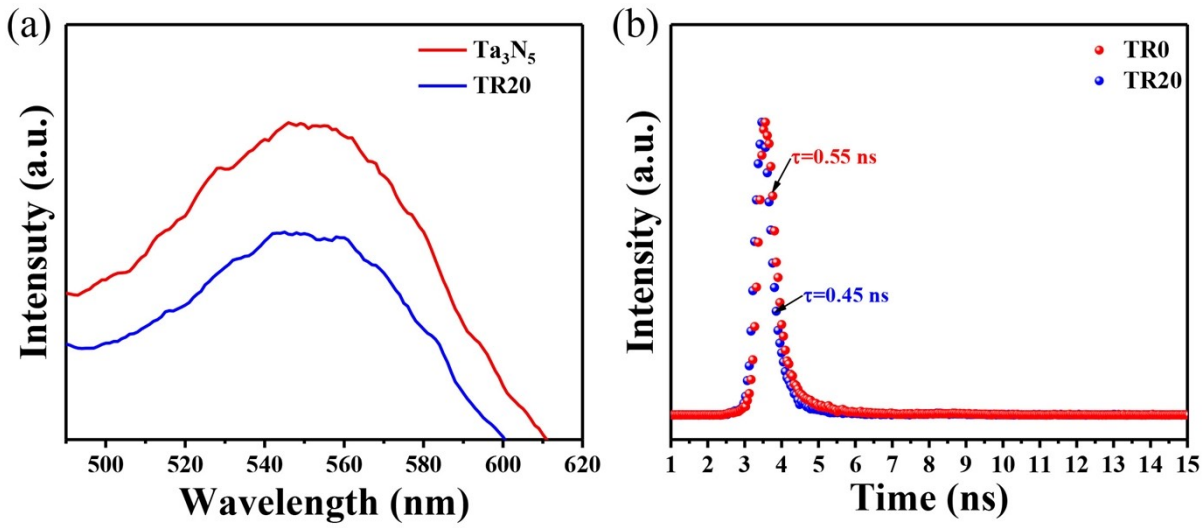

Fig. S9 (a-b) Steady state (a) and time-resolved (b) photoluminescence spectra of TR20, respectively.

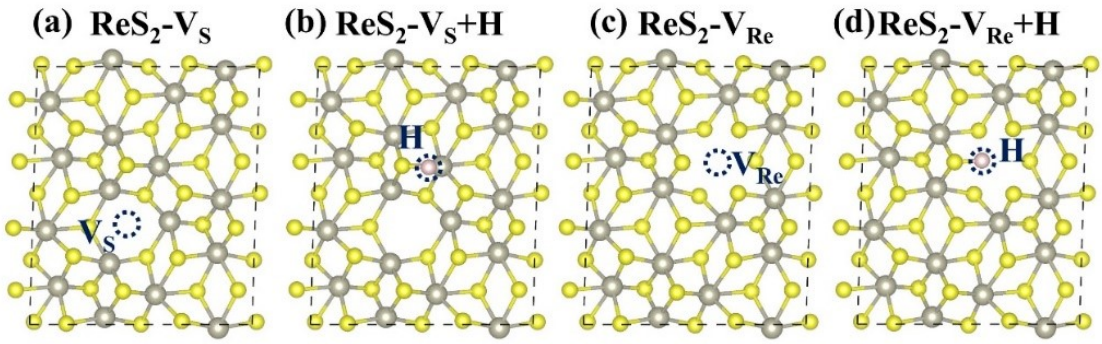

Fig. S10 (a, c) The optimized ReS_2 with S vacancy (V_S) (a) and Re vacancy (V_{Re}) (c), and (b, d) the corresponding H* adsorption around defects, respectively.

Discussion:

An exploration on the impact of defects on HER performance is investigated by DFT. Because H* is adsorbed on the surface of ReS_2, in order to exclude the influence of adsorption sites, we mainly compare the effect of defects between sole ReS_2 systems and Ta_3N_5@ReS_2 heterostructures with the H* adsorbed at the same sites. As show in Fig. S10a-d, some surface defects, *e.g.*, S vacancy (V_S) and Re vacancy (V_{Re}), are built in ReS_2 surface and Ta_3N_5@ReS_2 heterostructure, where the H* is absorbed at hollow site of among three S atoms closest to the defects. The results show that V_S could hardly improve the HER performance of Ta_3N_5@ReS_2 heterostructure, or even weaken that of ReS_2 surface (see Fig. 9f). In contrast, V_{Re} can significantly enhance the adsorption of H*, leading to a much smaller ΔG_{H^*} (0.14 for ReS_2-V_{Re} and 0.06 for Ta_3N_5@/ReS_2-V_{Re}) close to zero with enhanced HER performance. Owing to the higher electronegativity of S (2.58) than that of Re (1.90), the H* trends to be adsorbed with S atom. Besides, the appearance of one V_{Re} will inevitably break six Re-S bonds (Fig. S10c), which leads to the dangling bonds of S atoms with unpaired electron that could attract H* for electron pairing. Therefore, the V_{Re} brings an improved HER activity of ReS_2-based materials. What's more, the combination of Ta_3N_5 in the Ta_3N_5@ReS_2 systems could enhance the HER performance of sole ReS_2, regardless of the existed defects. Especially, Ta_3N_5@ReS_2-V_{Re}

exhibit better HER performance than both Ta_3N_5 and ReS_2-V_{Re}, representing the synergistic enhancement effect of Ta_3N_5, ReS_2 and V_{Re}.

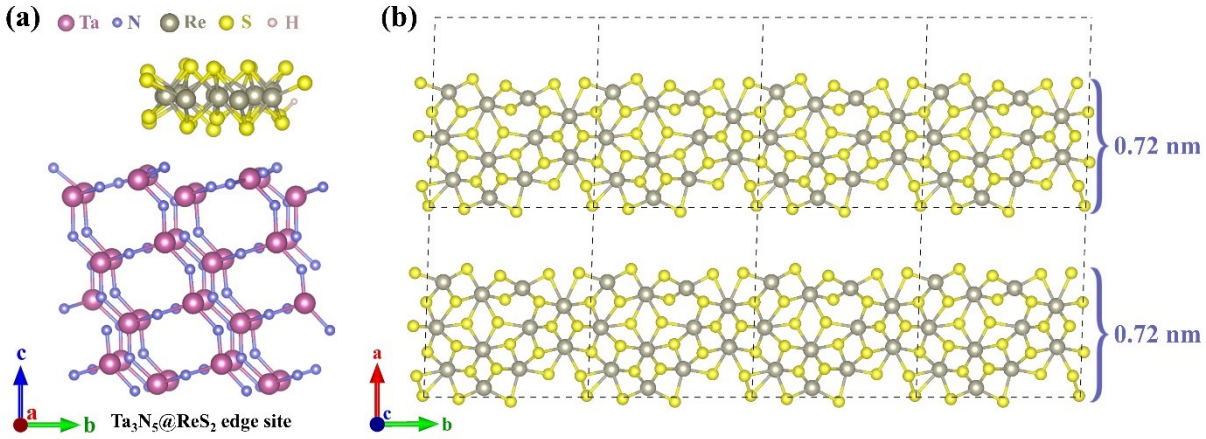

Fig. S11 The structures of Ta_3N_5 combined by incomplete ReS_2 with high-concentraion V_{Re} (a) and ReS_2 sheet with edges (b).

According to the DOS in Fig. 9g(IV), it seems that there are a lot of interface states within the midgap, which would become the center of carrier recombination. With the loss of Re atoms, many unsaturation S atoms at the edge of ReS_2, implying that there are lots of V_{Re} defects at the edge of ReS_2. Accordingly, it could be concluded that a small number of V_{Re} would enhance the adsorption of H* with thus improved HER performance (ΔG_{H^*} = 0.06 eV). However, too much V_{Re} would make the adsorption energy of H* be too high to desorb the H* with weakened HER performance (ΔG_{H^*} = -0.24 eV). In the real experiment, the ReS_2 sheet is > 10 nm, which is too large for DFT calculations. Here, we buit a ReS_2 sheet strucutral model with the size of 0.72 nm (see Fig. S11b), which is much smaller than that in real experiment to generate a much higher concentration of V_{Re}. If the concentration of V_{Re} are reduced by the edge passivation, the HER performance would get enhanced, implying that there might be a optimal defect concertation toward best HER performance.

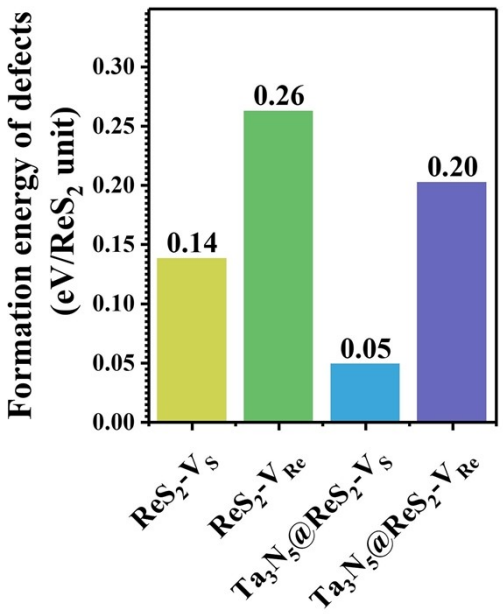

Fig. S12 The formation energies of the V_S and V_{Re} in sole ReS_2 surface and Ta_3N_5@ReS_2 heterostructure.

Table S1 The atomic ratio of the detected elements in EDX

element	Atom (%)
Ta	58.78
N	35.2
Re	2.1
S	3.92

Table S2 Comparison of activity for photocatalytic H_2 generation for some Ta_3N_5 based heterojunctions

Catalyst	Light source	Cocatalyst	Amount of H_2 ($\mu mol\ g^{-1}h^{-1}$)	AQE	*Ref.*
Ta_3N_5/ReS_2Uns	300W Xe lamp	/	739.4	0.102% at 420 nm	This work
$Ta_3N_5/CdIn_2S_4$	300W Xe lamp	3 wt% Pt	122.6	/	1
Ta_3N_5/PANI	300W Xe lamp (λ>410nm)	/	72.6	/	2
MoS_2/Ta_3N_5	300W Xe lamp	Pt	119.4	/	3
$SrTaO_2N/Ta_3N_5$	300W Xe lamp (λ>420nm)	4 wt% Pt	19.07	/	4
MgO/Mg-Ta_3N_5	300W Xe lamp (λ>400nm)	1 wt% Pt 2 wt% CoO_x	588	0.31% at 400 nm	5
Ta_3N_5/MoS_2	300W Xe lamp (λ>420nm)	/	565	0.882% at 420 nm	6
Ta_3N_5 Nanomeshes	Simulated sun light	1 wt% Pt	580	0.53% at 450 nm	7
$Ta_3N_5/SrTaO_2N$	300W Xe lamp (λ>420nm)	3 wt% Pt	77.31	/	8
$ZnIn_2S_4/Ta_3N_5$	300W Xe lamp	3 wt% Pt	834.86	/	9
Ta_3N_5-$WO_{2.72}$	150 W Xe lamp	Pt	516	/	10

References

1 Z. Peng, Y. Jiang, Y. Xiao, H. Xu, W. Zhang and L. Ni, Appl. Surf. Sci., 2019, 487, 1084-1095.
2 B. Niu and Z. Xu, J. Catal. , 2019, 371, 175-184.
3 M. Xiao, B. Luo, S. Thaweesak and L. Wang, Prog. Nat. Sci. Mater., 2018, 28, 189-193.
4 W. Zeng, S. Cao, L. Qiao, A. Zhu, P. Tan, Y. Ma, Y. Bian, R. Dong, Z. Wang and J. Pan, J. Colloid Interface Sci. , 2019, 554, 74-79.
5 M. Xiao, Z. Wang, B. Luo, S. Wang and L. Wang, Appl. Catal. B 2019, 246, 195-201.
6 L. Pei, Y. Yuan, J. Zhong, T. Li, T. Yang, S. Yan, Z. Ji and Z. Zou, Dalton Trans. , 2019, 48, 13176-13183.
7 M. Xiao, B. Luo, M. Lyu, S. Wang and L. Wang, Adv. Energy Mater., 2018, 8, 1701605.
8 X. Jia, W. Chen, Y. Li, X. Zhou, X. Yu and Y. Xing, Appl. Surf. Sci. , 2020, 514, 145915.
9 Y. Xiao, W. Zhang, Q. Xing, X. Feng, Y. Jiang, Y. Gao, H. Xu, J. Zhang, L. Ni and Z. Liu, Int. J. Hydrogen Energy, 2020, 45, 30341-30356.
10 W.-P. Hsu, M. Mishra, W.-S. Liu, C.-Y. Su and T.-P. Perng, Appl. Catal. B, 2017, 201, 511-517.